Organic & Biomolecular Chemistry

RSC Publishing

PAPER

View Article Online
View Journal | View Issue

Cite this: *Org. Biomol. Chem.*, 2013, **11**, 5642

The effect of the 4-amino functionality on the photophysical and DNA binding properties of alkyl-pyridinium derived 1,8-naphthalimides†

Swagata Banerjee, Jonathan A. Kitchen, Thorfinnur Gunnlaugsson* and John M. Kelly*

Received 20th February 2013,
Accepted 26th June 2013

DOI: 10.1039/c3ob40370j

www.rsc.org/obc

The synthesis and characterisation of two cationic pyridinium based 4-amino-1,8-naphthalimide derivatives (**2** and **3**) are described and compared to those of compound **1**. The photophysical properties of **2** and **3** are shown to vary greatly with the solvent polarity and H-bonding ability. The dimethylamino substitution in **3** results in a weak quantum yield of fluorescence emission due to faster non-radiative deactivation of the excited singlet state than that seen for **2**. As with **1**, the fluorescence of **2** was found to be enhanced in its 1 : 1 complex with 5′-adenosine-monophosphate (5′-AMP) while it was partially quenched in its complex with 5′-guanosine-monophosphate (5′-GMP). In contrast, the fluorescence of **3** was enhanced ('switched on') in the presence of both adenine and guanine rich sequences. Linear and circular dichroism studies showed that each of **1**, **2** and **3** binds to double-stranded DNA by intercalation. However, **2** and **3** do not show the preference for AT-rich DNA observed for **1**. Comparative fluorescence studies with double stranded DNA show that the emission of **3** was 16 times enhanced in its DNA bound form, suggesting potential use of this structure as a spectroscopic probe for studying nucleic acid structure.

Introduction

The development of small molecules capable of binding to canonical B-DNA and exhibiting anticancer activities is currently an active area of research.[1] In this context, 1,8-naphthalimide derivatives, originally developed by Braña and co-workers, represent an important family of DNA binders that show significant anti-tumour activities *in vitro* and *in vivo*.[1,2] In addition to their excellent DNA binding abilities, 1,8-naphthalimide derivatives display interesting photophysical properties, which are dependent on the nature, as well as the position, of any aryl substituents. The unsubstituted and the 3- and 4-nitro substituted naphthalimides possess high energy excited states, absorbing in the short wavelength region, while the 3- and 4-amino-1,8-naphthalimide derivatives absorb in the visible region (λ_{max} = 450 nm) and emit at longer (λ_{max} = 550 nm) wavelengths, with reasonably high quantum yields of emission in various organic and aqueous solvents.[3] The latter qualities are due to excited states that are characterised by a "push–pull" internal charge transfer (ICT) character,[3] arising from the presence of the electron-withdrawing imide and the electron donating amino moiety. This "push–pull" character becomes more efficient when the electron-donating group is in the 4-position of the naphthalene ring due to resonance stability. Due to their polarity sensitive emission properties and tunable redox properties, 4-amino-1,8-naphthalimide derivatives have been extensively explored for the development of sensors for biologically relevant ions,[4] molecules,[5] potential cellular imaging agents[6] and DNA binding molecules.[7] With the aim to develop bi-functional DNA binding agents, we have also reported the development of *N*-aminoalkyl[8] and bis-*N*-Ru(II) polypyridyl complexes[9] of 4-amino-1,8-naphthalimides, formed through the formation of a Tröger's base moiety.

Recently we reported a detailed study of the interaction of a pyridinium based 4-amino 1,8-naphthalimide **1** (Fig. 1) with 5′-AMP, 5′-GMP and DNA, which showed that the compound exhibits an enhanced fluorescence emission in the presence of 5′-AMP and DNA, while the fluorescence is quenched by 5′-GMP, indicating that the singlet excited state of the 4-amino-1,8-naphthalimide derivative can oxidise guanine but not adenine.[10] This study also showed that in contrast to what was reported for the unsubstituted compound,[11] the 4-amino-

School of Chemistry, Centre of Synthesis and Chemical Biology, and Trinity Biomedical Science Institute, University of Dublin, Trinity College Dublin, Dublin 2, Ireland. E-mail: jmkelly@tcd.ie, gunnlaut@tcd.ie;
Tel: +353 1 896 1947, +353 1 896 3459

†Electronic supplementary information (ESI) available: Figures ESI 1–10. CCDC 924757 and 924758. For ESI and crystallographic data in CIF or other electronic format see DOI: 10.1039/c3ob40370j

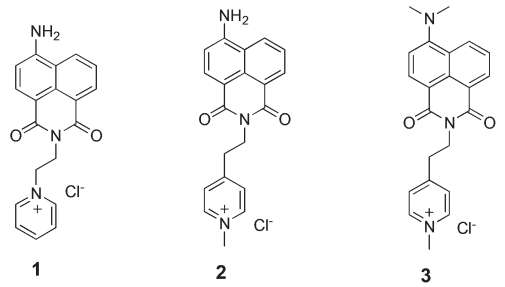

Fig. 1 Structures of **1–3**.

derivative **1** binds to DNA *via* intercalation and displays a strong preference for AT-rich sequences.[10] To further probe the binding of 4-amino-1,8-naphthalimides with DNA, we have synthesised two novel structurally related derivatives **2** and **3** (Fig. 1). These were designed to study the effects of (i) methyl substitution of the pyridine nitrogen on the imide side chain (while retaining the same spacer length as in **1**) and (ii) changing the 4-amino nitrogen substitution from a primary (*e.g.* **2**) to a tertiary amine (*e.g.* **3**) on the photophysical and DNA binding properties of such 4-amino-1,8-naphthalimide derivatives. Indeed we demonstrate that both these modifications have a significant effect on the interactions of **2** and **3** with nucleotides (5′-AMP, 5′-GMP) as well as DNA. This study shows that although **2** and **3** both contain a quaternised pyridine functional group, their binding behaviour with DNA is significantly different from that of **1**. Moreover, we demonstrate that **3** gives rise to a larger relative enhancement in the fluorescence emission upon binding to DNA than that seen for **2**, although the latter possesses a much higher quantum yield of fluorescence in its free unbound form. Hence, these simple structural modifications enabled us to fine-tune desirable properties that can be employed in the design of novel naphthalimide derivatives targeted to DNA with potential use as therapeutic and imaging agents.

Results and discussion

Design, synthesis and solid state characterisation of 2 and 3

Compound **2** was synthesised in three steps as shown in Scheme 1a. The first step involved condensation of 4-nitro-1,8-naphthalic anhydride with 4-(2-aminoethyl)pyridine in anhydrous toluene in the presence of triethylamine to give **5** in 47% yield, after basic aqueous workup and recrystallisation from hot ethanol. Reduction of **5** using hydrazine in methanol and 10% Pd/C gave compound **4** as a yellow solid in 94% yield. The final product **2** was then obtained as an iodide salt by reacting **4** with excess CH_3I in refluxing anhydrous acetone followed by purification by silica flash chromatography. Finally compound **2** as its Cl^- salt was obtained as a bright yellow solid in 93% yield.

Compound **3** was synthesised in a three step synthetic pathway as shown in Scheme 1b. The first step involved the conversion of 4-bromo-1,8-naphthalic anhydride into the

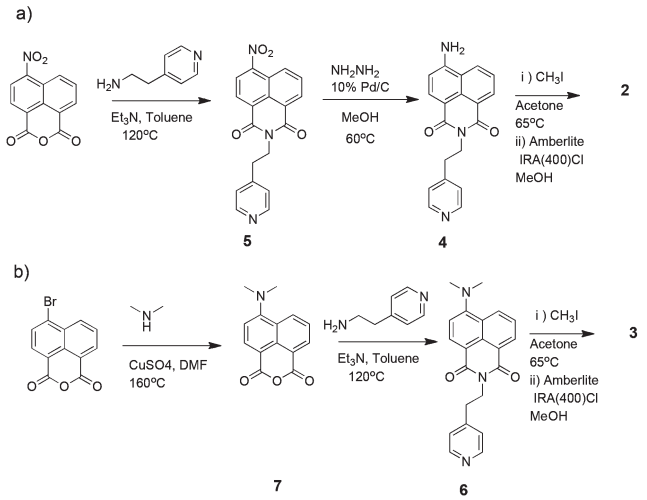

Scheme 1 Synthetic route for **2–3**.

4-*N*,*N*′ dimethyl analogue **7** using a modified literature procedure in the presence of $CuSO_4$ in DMF in 78% yield as a yellow solid.[12] Condensation of **7** with 4-(2-aminoethyl)-pyridine in anhydrous toluene in the presence of triethylamine yielded **6** in 56% yield, following aqueous workup and recrystallisation from methanol. Treating **6** with excess CH_3I in refluxing acetone solution, followed by purification using silica flash column chromatography, gave **3** as an orange solid in 40% yield. This product was then converted into its Cl^- salt using IRA(400) Cl-ion exchange resin.

Small yellow plate shaped crystals of **2** as the chloride salt suitable for X-ray diffraction were grown by slow evaporation of a methanolic solution. The low temperature (108 K) X-ray crystal structure showed that **2** crystallised in the triclinic space group $P\bar{1}$ (Fig. 2a) and contained one molecule of **2** with two interstitial water molecules in the asymmetric unit. The ethylene linker between the naphthalimide and pyridinium moieties adopts an *anti*-conformation. This is in contrast to what was previously observed for **1**, where the ethylene linker adopts a *gauche* conformation so that the pyridinium ring is oriented towards the naphthalimide. The pyridinium ring for **2** is not coplanar with the naphthalimide mean plane; instead it is angled at *ca.* 35° out of the expected coplanar arrangement. This is possibly a consequence of the weak, non-classical C–H hydrogen bonding interactions observed between the four pyridinium protons and chloride counter anions or interstitial water molecules (ESI†). Extensive π···π stacking interactions were observed between adjacent naphthalimide groups resulting in the head-to-tail arrangement of molecules (Fig. 2b). Packing interactions are primarily dominated by an extensive hydrogen-bonding network between the amino group and interstitial water protons as donors, and chloride, carbonyl oxygen atoms and water oxygen atoms as acceptors (see ESI†). The complete list of H bonding parameters observed in the crystal structure of **2** is detailed in ESI (ESI Table 3†).

Yellow coloured single crystals suitable for X-ray diffraction studies were also obtained by slow evaporation of an ethanolic

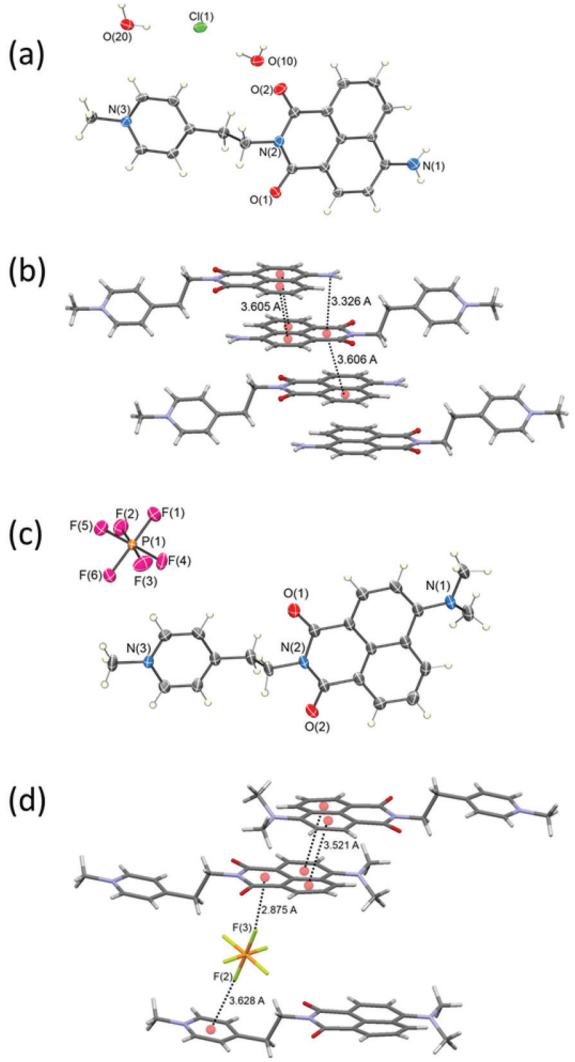

Fig. 2 (a) X-ray crystal structure of **2** as its Cl^- salt with thermal ellipsoids shown at 50% probability, (b) the packing of **2** showing the π···π interactions, (c) the X-ray crystal structure of **3** as its PF_6^- salt with thermal ellipsoids shown at 50% probability, and (d) the packing of **3** showing the anion···π and π···π interactions.

solution of **3** as the PF_6^- salt. The low temperature (100 K) crystal structure is shown in Fig. 2c. As is the case for **2**, the ethylene linker in **3** adopts an *anti* conformation. The pyridinium ring and the naphthalimide ring assume an almost coplanar orientation in the crystal structure. The NMe_2 group was found to be in a slightly twisted conformation with (C_{naph}–C_{naph}–N–Me) torsion angles of *ca.* −5° and 42° for methyl C20 and methyl C21 respectively. The packing is governed by strong anion···π interactions[13] between the fluorine atom of the PF_6^- ion and the imide ring (F3···centroid distance 2.875 Å) and π···π stacking interactions between the naphthalene rings on adjacent molecules (centroid···centroid distance 3.521 Å) resulting in head-to-tail organisations of the naphthalimide molecules. In addition there is a very weak anion···π interaction between the pyridinium ring and the PF_6^- (F2···centroid = 3.628 Å) giving an overall π···anion···π interaction (Fig. 2d).

UV/visible and fluorescence studies of 2 and 3

Having fully characterised the new analogues **2** and **3**, their photophysical properties were first examined in aqueous phosphate buffer. **2** displayed a broad ICT absorption band centred at 435 nm (ε = 13 800 M^{-1} cm^{-1}) and high energy π–π* transitions at *ca.* 250 nm (26 150 M^{-1} cm^{-1}). Excitation of **2** at 435 nm resulted in a broad emission band centred at 550 nm (Fig. 3a).

In contrast to **2**, the absorption band for the *N*,*N*′-dimethyl analogue **3** was shifted to a longer wavelength (λ_{max} = 450 nm, ε = 11 290 M^{-1} cm^{-1}) with a shoulder at *ca.* 400 nm, which was not observed for the 4-amino analogue (Fig. 3b). The shoulder centred around 400 nm observed in the absorption spectrum of **3** was found to be present in a range of concentrations investigated (2 → 100 μM) and to obey the Beer–Lambert law in this concentration range (ESI†). However 600 MHz ^{1}H NMR analysis of **3** in D_2O (ESI†) showed that the protons from the naphthalene ring exhibited a significant downfield shift on changing the concentration from 1 mM to 10 μM, indicative of aggregation at higher concentration, even though the UV/vis absorption spectrum of **3** remained practically unchanged in this concentration range. Based on the ^{1}H NMR data, the possibility of some aggregation in aqueous solution cannot therefore be completely ruled out even at 10 μM concentration.

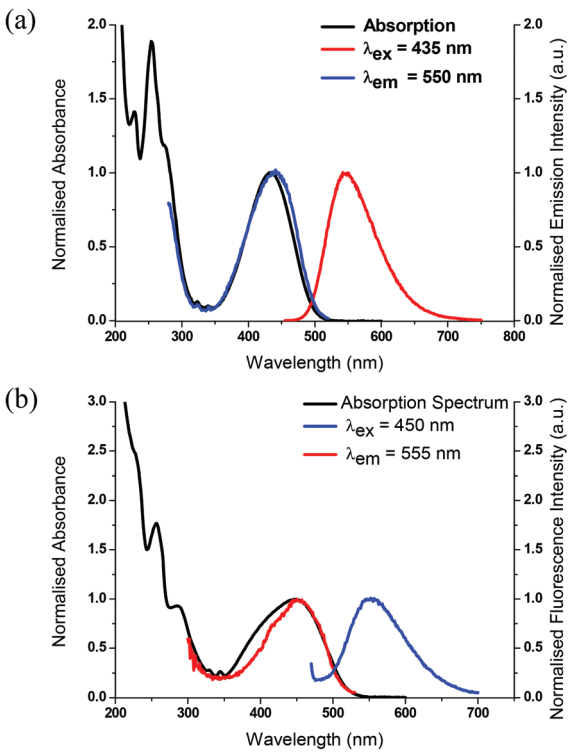

Fig. 3 Normalised UV/vis absorption spectrum and fluorescence excitation and emission spectra of (a) **2** (7.1 μM) and (b) **3** (7.0 μM) in 10 mM phosphate buffer (pH 7.0).

Table 1 Absorption and fluorescence emission data for **2** and **3** in different solvents

	λ_{max} (Abs) (nm)					λ_{max} (Flu) (nm)				
	BuOH	i-PrOH	*n*-PrOH	EtOH	H_2O	BuOH	i-PrOH	*n*-PrOH	EtOH	H_2O
1[a]	445	444	444	440	436	530	532	534	536	552
2	443	443	441	439	435	525	523	527	528	550
3	425	426	426	427	450	527	527	529	532	555

[a] Data for **1** were incorporated from ref. 10 for comparison.

Excitation of **3** at 450 nm resulted in a broad emission band centred at 555 nm (Fig. 3b). The emission band was not affected by changing the excitation wavelength from 450 nm to 400 nm. The shoulder at 400 nm observed in the UV/vis absorption spectrum of **3** was not present in the excitation spectrum recorded in aqueous solution using λ_{em} = 555 nm, suggesting that the emission arises from the monomeric species in solution.

To aid in understanding the contrasting behaviour of **2** and **3** in aqueous solution, the absorption and emission spectra of **2** and **3** were recorded in different alcoholic solvents (Table 1). In all the solvents studied, compound **2** exhibited a broad absorption band, which showed a slight blue shift (*ca.* 8–9 nm) on moving from the less polar butanol to the highly polar water (Fig. 4a). In the case of **3**, the absorption maxima remained relatively unchanged between various alcohols but showed a large (*ca.* 23 nm) red shift on changing solvent from ethanol to water (ESI†). Additionally, in all alcoholic solvents, the absorption band of the dimethyl analogue **3** is blue shifted compared to **2**, whereas in water the band for **3** is significantly red shifted relative to **2**. The behaviour of **3** in all alcoholic solvents may be explained if the dimethylamino (NMe_2) moiety is twisted relative to the naphthalimide ring such that the amino nitrogen cannot participate in the ICT process as efficiently as in the 4-amino analogues. The solid-state structure of **3** also revealed that the NMe_2 group is slightly twisted relative to the naphthalene ring thereby supporting the spectroscopic data. The considerably red shifted absorption band of **3** in aqueous media suggests the possibility of aggregation, which is possibly a consequence of the presence of two additional hydrophobic methyl groups.

In contrast to the absorption spectra, an increase in the polarity of the media resulted in red shifts in the fluorescence bands for both **2** and **3** and a decrease in fluorescence quantum yield and lifetime on moving from butanol to water (*cf.* Table 2), a behaviour characteristic of an ICT excited state.[14] Representative spectra for **2** are shown in Fig. 4b and the fluorescence maxima in each solvent are summarised in Table 1.

The radiative and non-radiative rate constants were calculated for **2** in various solvents from the measured value of Φ_F and τ_F and are presented in Table 3. This shows that the magnitude of the radiative decay constant (k_r) is not significantly altered with an increase in polarity of the alcohol, while the non-radiative decay constant (k_{nr}) increased substantially

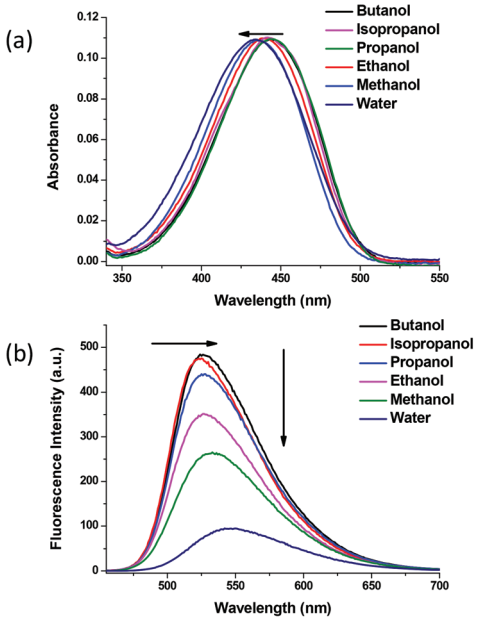

Fig. 4 UV/vis absorption and fluorescence spectra of **2** in different solvents.

between butanol and ethanol. This increase in k_{nr} on moving towards more polar and H-bonded solvents accounts for the decrease in Φ_F.

Compound **3** has much lower fluorescence quantum yields compared to **2** in all the solvents studied (*cf.* Table 2), making fluorescence lifetime studies more difficult. In butanol, analysis by bi-exponential kinetics showed that the dominant lifetime was 0.28 ns (93%). This lifetime must be regarded as an upper limit, as it is obtained by deconvolution of the exciting pulse (1.2 ns). This would indicate that the non-radiative decay of the excited state is $>3 \times 10^9$ s^{-1}. A more detailed study of the nature of the non-radiative processes in **3** will require picosecond measurements.

In a related study, Saha *et al.* proposed that an increased rate of inversion of the amino nitrogen can also influence the k_{nr} value in a series of 4-amino-1,8-naphthalimide[14e] and 4-aminonitrobenzoxadiazole derivatives.[14f] Glusac and co-workers have also reported that in the optimised excited state geometry of 4-*N*,*N*′-dimethylamino-1,8-naphthalimide, the 4-substituent is at a 90° angle relative to the naphthalene ring.[15a] Such twisted excited states are more stabilised in highly polar solvents. These authors also reported the

Table 2 Fluorescence quantum yield (ϕ_F) and fluorescence lifetime (τ_F) of **2** and **3** in various solvents (λ_{ex} = 458 nm for fluorescence lifetime measurements)

	ϕ_F					τ_F (ns)				
	BuOH	i-PrOH	*n*-PrOH	EtOH	H_2O	BuOH	i-PrOH	*n*-PrOH	EtOH	H_2O
1[a]	0.40	0.29	0.23	0.16	0.08	5.1	3.9	3.2	2.6	2.2
2	0.51	0.50	0.47	0.37	0.11	8.4	8.2	7.8	7.3	3.1
3	0.015	0.013	0.012	0.007	0.001	—[b]	—[b]	—[b]	—[b]	—[b]

[a] Data for **1** from ref. 10. [b] Fluorescence decay could not be reliably measured.

Table 3 Radiative (k_r) and non-radiative decay constants (k_{nr}) of **2** in various solvents

	k_r ($\times 10^7$ s^{-1})					k_{nr} ($\times 10^7$ s^{-1})				
	BuOH	i-PrOH	*n*-PrOH	EtOH	H_2O	BuOH	i-PrOH	*n*-PrOH	EtOH	H_2O
1[a]	7.8	7.4	7.2	6.1	3.6	12	18	24	32	40
2	6.0	6.1	6.0	5.1	3.6	5.8	6.1	6.8	8.6	29

[a] Data for **1** from ref. 10.

shortening of fluorescence lifetime of 4-*N*,*N*′-dimethylamino-1,8-naphthalimide with increasing solvent polarity in a manner similar to that observed in the case of **3**. It has been proposed that the rate of the twisting process is enhanced with an increase in solvent polarity and consequently results in a decrease in the quantum yield of emission and lifetime of the excited state. A similar mechanism might be responsible for the observed photophysical behaviour of **3**. However, the absence of dual emission in this case suggests that the twisted excited state is presumably non-fluorescent as observed previously for the 4-*N*,*N*′-dimethylaminophthalimide derivatives.[15b] A characteristic shoulder in the absorption spectrum similar to that observed for **3** was also reported for a bichromophoric system incorporating an *N*,*N*′-dimethylaniline and a decahydroacridinedione.[16] However, this compound showed two fluorescence bands in aprotic solvents that were attributed to two different conformations of the ground state, giving rise to closely lying local and charge transfer excited states. As only one emission band is observed for **3** in all the solvents studied, a similar mechanism is unlikely here.

Since **2** and **3** exhibit significant solvatochromism and as their emission quantum yields are strongly dependent on solvent polarity, the binding of these derivatives to nucleotide monophosphates and DNA is expected to cause substantial changes in the photophysical properties of the ligands.

Interaction with mononucleotides

Ground state interactions with mononucleotides. The interactions of **2** and **3** with mononucleotides were initially investigated, and the changes observed in the UV/vis spectrum of **2** in the presence of 5′-GMP are shown in Fig. 5a. The addition of 5′-GMP to the solution of **2** in 10 mM phosphate buffer (pH 7.0) resulted in a decrease in the long-wavelength absorption band at 435 nm and *ca.* 7 nm red shift in λ_{max} with the concomitant formation of a single isosbestic point at 460 nm. Similar changes were also observed in the ground state spectrum of **2** in the presence of 5′-AMP (ESI†). These observations suggest the formation of spectroscopically distinct free and 5′-XMP (X = A/G) bound naphthalimide species in solution, which has been previously observed for other 1,8-naphthalimide derivatives and has been attributed to naphthalimide–nucleotide stacking interactions.[10,17] The changes in the UV/vis absorption spectra of **3** in the presence of 5′-AMP and 5′-GMP were significantly different from those observed for **2**, since with increasing concentration of the mononucleotide, the band centred at 450 nm showed a *ca.* 8–9 nm red shift. However, the absorbance at 450 nm did not decrease significantly (Fig. 5c). Additionally, the absorbance at 400 nm corresponding to the shoulder decreased significantly and the shoulder feature disappeared at high concentrations of 5′-XMP. However, the decrease in absorbance at 400 nm did not reach a plateau even at very high concentrations of 5′-GMP (50 mM). The decrease in absorbance at 400 nm in the presence of 5′-GMP is indicative of naphthalimide–5′-GMP stacking interaction. The lack of a plateau in the binding isotherm suggests a weak interaction between **3** and 5′-GMP. This possibly results from a slightly twisted conformation of the dimethyl amino group relative to the plane of the naphthalimide ring, which can interfere with the binding of 5′-GMP to the planar surface of the naphthalimide ring. Assuming a 1 : 1 stoichiometry of binding, the binding constants of **2** and **3** were calculated for 5′-AMP and 5′-GMP using the Scatchard equation[18a] and the non-linear model of Deranleau[18b] and the results are given in Tables 4 and 5. This showed that **1** and **2** display comparable binding affinity towards both purine nucleotides. However, the binding constants for the association of **3** with 5′-AMP and 5′-GMP were significantly lower and were comparable to the unsubstituted compound[17b] suggesting that the 4-amino group is possibly involved in the interaction with mononucleotides. Additionally, the slightly

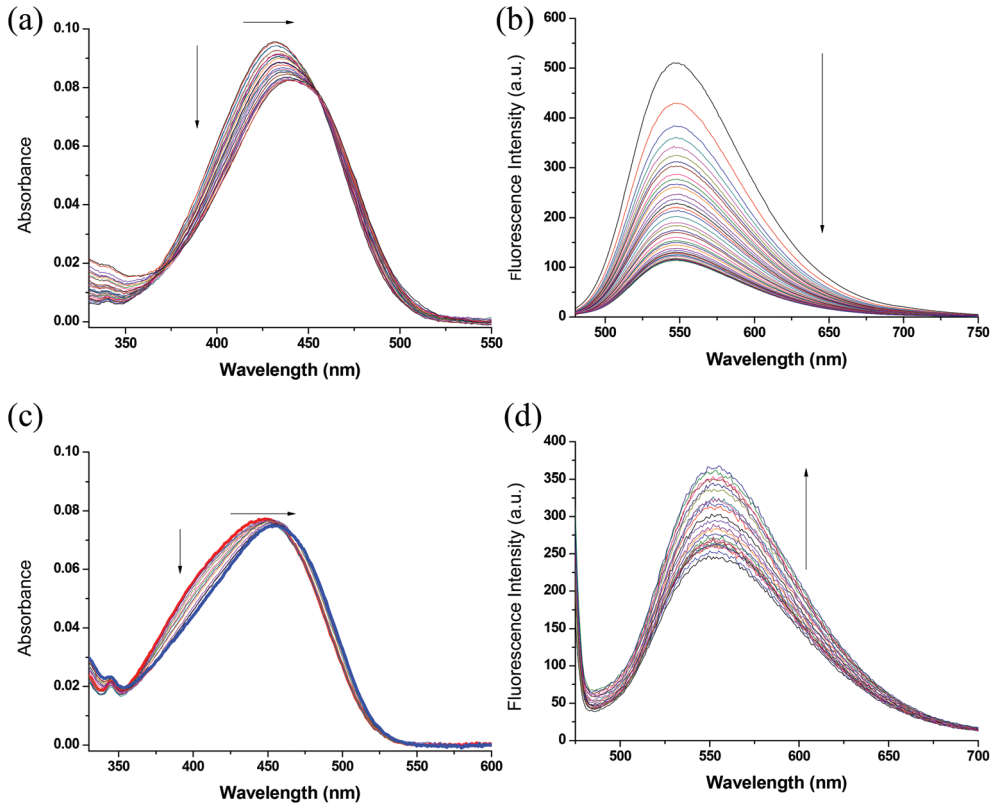

Fig. 5 Changes in the (a) absorption spectrum and (b) fluorescence spectrum (λ_{ex} = 460 nm) of **2** (7.2 μM) and changes in the (c) absorption spectrum and (d) fluorescence spectrum (λ_{ex} = 450 nm) of **3** (6.8 μM) in the presence of increasing concentration of 5′-GMP (0–50 mM) in 10 mM phosphate buffer pH 7.0.

Table 4 Summary of absorption parameters for the interaction of **2** and **3** with 5′-GMP

		1[a]	**2**	**3**
λ_{max} (Abs) (free) (nm)		436	435	450
λ_{max} (Abs) (bound) (nm)		442	442	458
$\Delta\lambda$ (nm)		+6	+7	+8
% Hypochromism		12	11	—[b], 20[c]
Isosbestic point (nm)		470	460	455 (not well defined)
K (M^{-1})	Scatchard	117 ± 11	100 ± 5	—[d]
	Deranleau	135 ± 5	125 ± 8	—[d]

[a] Data for **1** from ref. 10. [b] No decrease in absorbance at λ_{max} = 450 nm. [c] Hypochromism at 400 nm. [d] Data could not be fitted due to the lack of an end point.

Table 5 Summary of absorption parameters for the interaction of **2** and **3** with 5′-AMP

		1[a]	**2**	**3**
λ_{max} (Abs) (free) (nm)		436	435	450
λ_{max} (Abs) (bound) (nm)		445	446	460
$\Delta\lambda$ (nm)		+10	+11	+10
% Hypochromism		19	13	—[b], 27[c]
Isosbestic point (nm)		463	460	455 (not very clear)
K (M^{-1})	Scatchard	K_1 = 138 ± 10 K_2 = 37 ± 5	100 ± 5	70 ± 3
	Deranleau	K_1 = 155 ± 7 K_2 = 35 ± 5	125 ± 8	66 ± 4

[a] Data for **1** from ref. 10. [b] No decrease in absorbance at λ_{max} = 450 nm. [c] Hypochromism at 400 nm.

twisted structure of the *N*,*N*′-dimethyl amino group in **3** might also affect the interaction with the mononucleotides.

Singlet excited state interaction of 2 and 3 with mononucleotides. Having shown the ground state interactions of **2** and **3** with mononucleotides, we next investigated the changes in the fluorescence emission spectra of **2** and **3** in the presence of 5′-AMP and 5′-GMP. In the case of **2**, the fluorescence intensity initially decreased at low concentrations of 5′-AMP (0–0.9 mM) and then increased by a factor of 1.5 with further addition of 5′-AMP (ESI†). The fluorescence intensity for **3** increased by a factor of four in the presence of increasing concentrations of 5′-AMP (0 → 100 mM). However, the changes in fluorescence of **3** did not reach a plateau at higher concentration of 5′-AMP unlike that observed for **2**. This could be a consequence of the weaker affinity of **3** towards 5′-AMP as determined by the UV/vis absorption titration. The increase in relative quantum yield of emission of both compounds in the presence of 5′-AMP can be attributed primarily to a decrease of the rate of non-radiative decay processes in the complex, where the ligand is less accessible to solvent molecules and also is in a relatively more rigid orientation. Similar changes in non-radiative decay processes have been reported for the interaction of various

porphyrin[19] and ethidium bromide derivatives[20] and 4-amino-1,8-naphthalimide **1** with nucleobases and DNA.[10]

In contrast to what was observed with 5′-AMP, the addition of 5′-GMP (up to 50 mM) caused *ca.* 75% quenching of the emission intensity of **2** (λ_{ex} = 460 nm), accompanied by a *ca.* 2 nm blue shift in the peak position (Fig. 5b). This can be attributed to photoinduced electron transfer (PET) occurring from guanine to the excited 4-amino naphthalimide derivative, as has been previously observed for other naphthalimide derivatives.[10,17] Quenching of the emission intensity of **2** at a lower concentration of 5′-GMP occurs in a 1 : 1 complex. The residual fluorescence observed at very high concentrations of 5′-GMP, where the ligand should be mostly bound, can be explained by considering fluorescence emission from the NI : 5′-GMP complexes. At very high concentration of 5′-GMP, the possibility of collisional quenching cannot be ruled out. In contrast to what was observed for **2**, the emission intensity of **3** increased almost linearly with increasing 5′-GMP concentration (0 → 50 mM) and did not reach a plateau at high concentration of 5′-GMP (Fig. 5d). Stacking interactions of **3** with mononucleotides can provide some extent of a rigid environment, which reduces the extent of non-radiative deactivations operating in aqueous solution and therefore can enhance the fluorescence quantum yield. The absence of any plateau in the binding isotherm indicates weak interaction between **2** and 5′-GMP, in agreement with the ground state absorption data.

Interaction with salmon testes (st)-DNA

Ground state interactions. The interactions of **2** and **3** with st-DNA were investigated from the changes in the UV/vis spectra of the ligands in the presence of DNA (Fig. 6a). In both cases the addition of st-DNA resulted in a large hypochromicity and red shift of the ICT absorption band, accompanied by the formation of a single isosbestic point at *ca.* 480 nm for all DNA/ligand (P/D) concentrations suggesting the presence of only two spectroscopically distinct species, *i.e.* the DNA bound and the free ligand. For **3**, absorbance at 400 nm corresponding to the shoulder decreased by *ca.* 62%. Similar changes in the absorption spectra have been observed for **1**[10] and various other 1,8-naphthalimides,[11,17,21] where the hypochromicity of the naphthalimide absorption band has been suggested due to intercalation of the planar naphthalimide ring between the stacked DNA bases. The changes in absorbance were fitted to the non-cooperative model of McGhee and von Hippel[22] to determine the binding constant, which showed that in 10 mM phosphate buffer solution the intrinsic binding constants for the association of **2** and **3** with st-DNA were found to be of the order of 10^5 M^{-1} (Fig. 6a inset and Table 6), which are comparable to the affinity of phenothiazine dyes for DNA[23] and naphthalimides fused with heterocyclic rings.[24] Interestingly, the presence of the dimethyl substitution on the 4-amino nitrogen did not appear to have any significant effect on the DNA binding affinity of **3**, in contrast to what was observed for the mononucleotides.

Excited state interactions with st-DNA. In the presence of st-DNA, the fluorescence intensity of each of **1**, **2** and **3** is enhanced concomitant with a blue shift in λ_{max} (Fig. 6b). However, the extent of the fluorescence enhancement and the shift in λ_{max} were very different for each naphthalimide–DNA pair. Whereas for **1** the fluorescence quantum yield increased steadily with increasing concentration of st-DNA, reaching a plateau with a quantum yield enhancement by a factor of 2.0,[10] the behaviour of **2** was strikingly different. Here the emission intensity of the ICT band (λ_{max} = 550 nm) initially increased by a factor of 1.6, reaching a maximum at a P/D ratio of *ca.* 17, accompanied by a *ca.* 11 nm blue shift in λ_{max}. Further increase in DNA concentration (P/D 20 → 55) resulted in a decrease of the emission intensity (Fig. 6b inset) and an additional 3 nm blue shift in λ_{max}. This total blue shift of

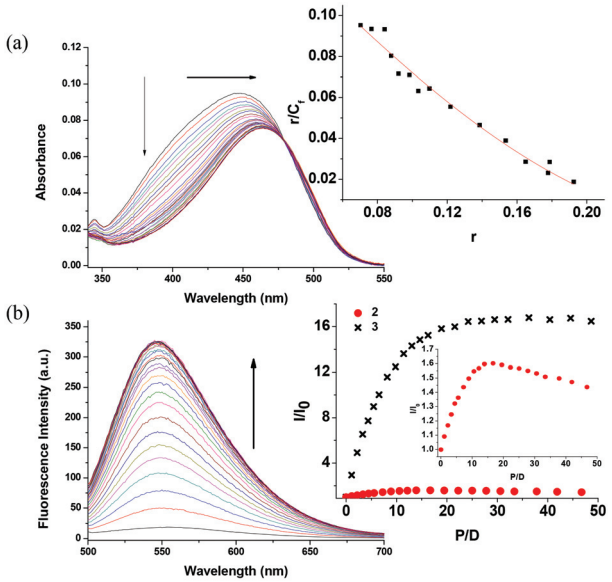

Fig. 6 (a) Changes in the UV/vis absorption spectra of **3** (7.8 μM) in the presence of increasing concentration of st-DNA (0–438 μM) in 10 mM phosphate buffer (pH 7.0). Inset: plot of r/C_f *vs.* r (■) and fit (—) to the non-cooperative model of McGhee and von Hippel. (b) Changes in the fluorescence spectra of **3** (7.8 μM) in the presence of increasing concentration of st-DNA (0–438 μM) in 10 mM phosphate buffer (pH 7.0) (λ_{ex} = 480 nm). Inset: plot of I/I_0 *vs.* DNA nucleotide phosphate/ligand (P/D) for **2** and **3**.

Table 6 Summary of binding parameters obtained from the absorption spectra of **1–3** in the presence of st-DNA in 10 mM phosphate buffer (pH 7.0)

	1[a]	**2**	**3**
λ_{max} (Abs) (nm) (free)	436	435	450
λ_{max} (Abs) (nm) (bound)	447	445	465
$\Delta\lambda$ (nm)	+11	+10	+15
% Hypochromism	44	44	22[b], 62[c]
Isosbestic point (nm)	480	480	480
Bound P/D	20	22	25
K ($\times 10^5$ M^{-1})	1.85 ± 0.05	1.38 ± 0.05	(1.49 ± 0.10)[b] (1.55 ± 0.05)[c]
n (bp)	2.65 ± 0.22	2.43 ± 0.05	(3.05 ± 0.25)[b] (3.40 ± 0.08)[c]

[a] Data for **1** from ref. 10. [b] Measured using absorbance at 450 nm. [c] Measured using absorbance at 400 nm.

14 nm may be contrasted with the more modest 5 nm shift of **1**. The biphasic behaviour for **2** is presumably indicative of multiple binding sites. One possibility is that the complex has a sequence preference and will then seek out a preferred site at a higher P/D ratio. However studies with polynucleotides, described below, suggest that this is probably not the case. Another possibility is that at a low P/D ratio there is interaction between the complexes (probably involving stacking), which is undone when more DNA is added. It would also be necessary to suppose that the dimers or aggregates were more fluorescent than the isolated DNA-bound naphthalimide and such behaviour has been proposed for some ruthenium polypyridyl complexes.[25] Biphasic behaviour is maintained upon raising the ionic strength by the addition of 100 mM NaCl (ESI†) indicating that the effect is not merely electrostatic in nature.

Fluorescence enhancement was much more pronounced with **3**, showing a *ca.* 16 fold increase in the emission intensity when fully bound to st-DNA (Fig. 6b). This behaviour is consistent with the location of the ligand in a less polar and more rigid site, where it is less accessible to water and therefore less susceptible to non-radiative decay. As noted above, the dimethyl substitution on the 4-amino nitrogen increases the non-radiative deactivation of the excited singlet state in **3** probably by rotation/twisting of Aryl–N bonds and inversion of amino nitrogen compared to **2**. These internal motions are expected to be significantly reduced when bound to DNA, resulting in an enhancement of the fluorescence quantum yield.[26]

Interaction with synthetic polynucleotides

As before, the changes in the UV/vis absorption spectra of **2** (Fig. 7a and 7b, respectively) and **3** (ESI†) with increasing concentrations of poly(dA–dT)$_2$ and poly(dG–dC)$_2$ were monitored. In the presence of either of the polynucleotides, a large hypochromicity was observed for the ICT absorption band of both **2** and **3** accompanied by a significant red shift in the λ_{max}. The equilibrium binding constants for the association of the naphthalimides with polynucleotides were determined from the fit of the absorbance data to the non-cooperative model of McGhee and von Hippel and are summarised in Table 7. This shows that both **2** and **3** showed comparable binding affinities for AT and GC rich sequences. This contrasts with the behaviour reported for the pyridinium based 4-amino-1,8-naphthalimide derivative **1**, which shows a strong

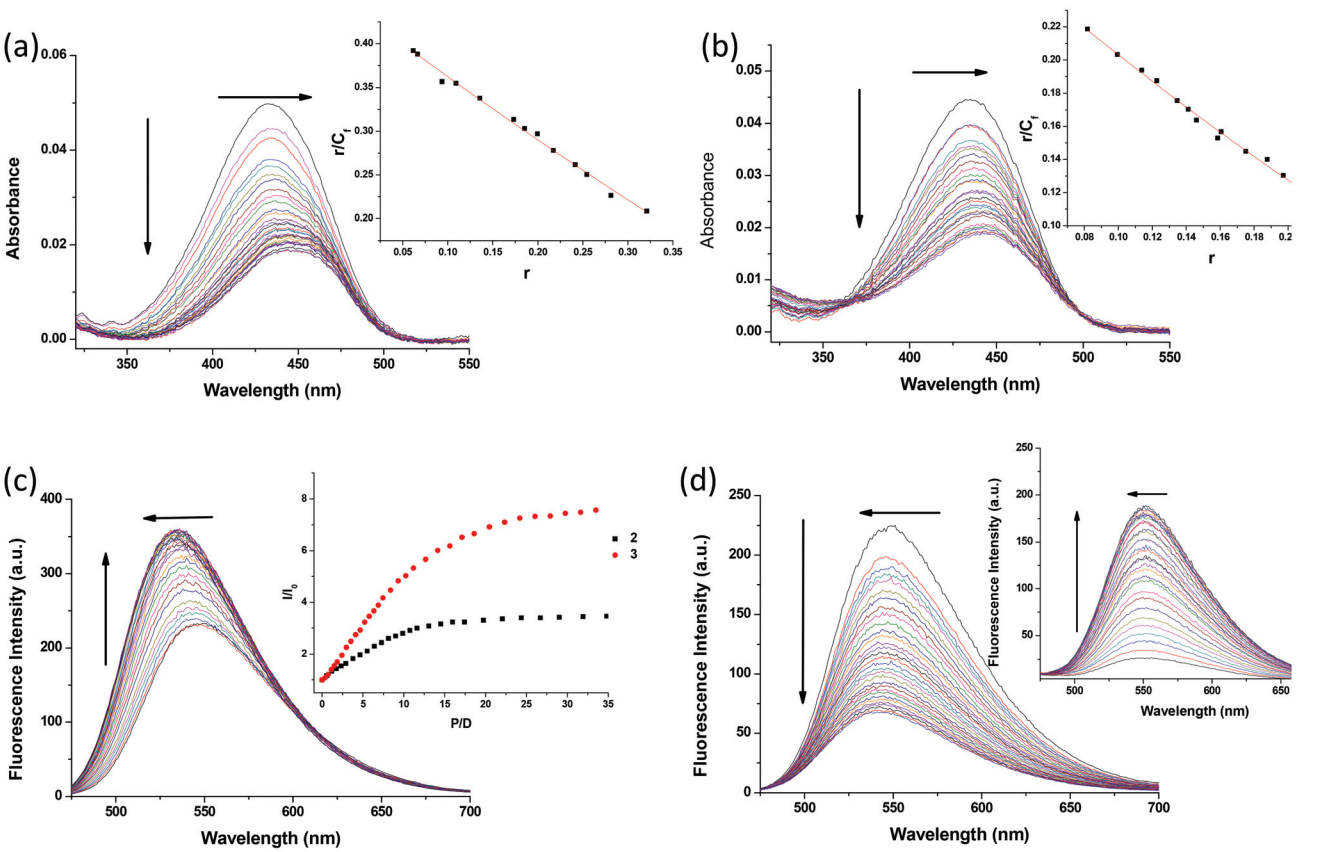

Fig. 7 The UV/vis absorption spectra of (a) **2** (4.0 μM) in the presence of increasing concentration of poly(dA–dT)$_2$ (0–140 μM); (b) **2** (4.0 μM) in the presence of increasing concentration of poly(dG–dC)$_2$ (0–165 μM) in 10 mM phosphate buffer (pH 7.0); inset a and b: plot of r/C_f *vs.* r and best fit (—) to the McGhee–von Hippel model for the titration of **2** with poly(dA–dT)$_2$ and poly(dG–dC)$_2$ respectively; (c) changes in the fluorescence spectra of **2** (4.0 μM) in the presence of poly(dA–dT)$_2$ (0–140 μM) (λ_{ex} = 435 nm); inset c: plot of I/I_0 *vs.* P/D for **2** and **3** respectively in the presence of poly(dA–dT)$_2$; (d) changes in the fluorescence spectra of **2** (4.0 μM) in the presence of increasing concentration of poly(dG–dC)$_2$ (0–165 μM). (λ_{ex} = 435 nm); inset d: changes in the fluorescence spectra of **3** (5.2 μM) in the presence of increasing concentration of poly(dG–dC)$_2$ (0–190 μM). (λ_{ex} = 450 nm) in 10 mM phosphate buffer (pH 7.0).

Table 7 Summary of binding parameters obtained from the absorption spectra of **1–3** in the presence of polynucleotides in 10 mM phosphate buffer (pH 7.0)

	1[a]		**2**		**3**	
	$(dA–dT)_2$	$(dG–dC)_2$	$(dA–dT)_2$	$(dG–dC)_2$	$(dA–dT)_2$	$(dG–dC)_2$
λ_{max} (Abs) (nm) (free)	436	436	435	435	450	450
λ_{max} (Abs) (nm) (bound)	447	445	447	447	463	462
$\Delta\lambda$ (nm)	+11	+9	+12	+12	+13	+12
% Hypochromism	49	52	57	57	17, 52[b]	12, 34[b]
Isosbestic point (nm)	480	—	—	—	—	—
Bound P/D	11	50	15	25	13	18
K ($\times 10^5$ M^{-1})	5.15 ± 0.10	0.82 ± 0.02	4.35 ± 0.01	2.87 ± 0.10	5.32 ± 0.02[b] 4.80 ± 0.03[c]	3.21 ± 0.05[b] 3.00 ± 0.03[c]
n (bp)	2.54 ± 0.12	3.62 ± 0.09	1.36 ± 0.02	2.20 ± 0.07	1.70 ± 0.10[b] 1.96 ± 0.05[c]	3.10 ± 0.10[b] 2.88 ± 0.09[c]
λ_{max} (Flu) (nm) (free)	552	552	550	550	555	555
λ_{max} (Flu) (nm) (bound)	547	544	535	543	537	552
$\Delta\lambda$ (nm)	−5	−8	−15	−7	−18	−3
I/I_0	2	0.70	3.5	0.74	7.5	8.5

[a] Data for **1** from ref. 10. [b] Measured using absorbance at 450 nm. [c] Measured using absorbance at 400 nm.

preference for AT rich sequences.[10] The comparable binding affinities of **2** and **3** toward AT and GC rich sequences possibly originate from the presence of an additional methyl group on the pyridyl nitrogen, which might result in better binding to both AT and GC sequences.

The changes in fluorescence intensity of **2** in the presence of increasing concentrations of poly$(dA–dT)_2$ are shown in Fig. 7c. Similar to what was observed for 5′-AMP, the emission of **2** was enhanced by a factor of 3.5, with a 15 nm blue shift in λ_{max} in the presence of poly$(dA–dT)_2$. Compound **3** also showed a *ca.* 7.5 fold enhanced fluorescence in the presence of poly$(dA–dT)_2$ and a 18 nm blue shift in λ_{max} (Fig. 7c inset and Table 7).

A different behaviour is found for poly$(dG–dC)_2$, where the fluorescence of **2** is quenched upon binding (Fig. 7d). This is consistent with PET, due to the oxidation of guanine by the singlet excited state of **2**. In contrast with this, the fluorescence intensity of **3** was enhanced by a factor of 8.5 in the presence of poly$(dG–dC)_2$ (Fig. 7d inset and Table 7). The enhanced fluorescence of **3** in the presence of GC rich sequences suggests that the excited state of **3** is much less oxidising than **1** and **2**, presumably due to the presence of the electron-donating *N*,*N*′-dimethyl amino group.

Thermal melting assay

The thermal melting curves of st-DNA (150 μM) in the presence of **2** and **3** are shown in Fig. 8. In the absence of any ligand, the T_m value for st-DNA was found to be (68 ± 0.5) °C. In the presence of ligands **2** and **3** (P/D = 10), moderate stabilisation of st-DNA was observed, indicated by a *ca.* 5–6° increase in the DNA melting temperature of st-DNA in a 10 mM buffer solution. It is perhaps significant that the extent of stabilisation is smaller than the effect observed for well-established intercalators such as ethidium bromide (ΔT_m > 10°).[27] However, such a moderate stabilisation has been observed previously for other mononaphthalimide based DNA intercalators and perhaps suggests a weaker intercalation efficiency of **2** and **3**.[8,10]

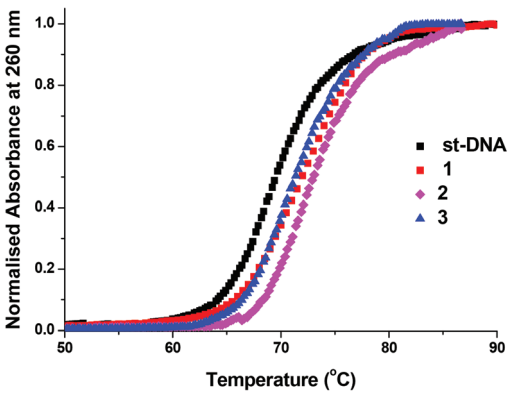

Fig. 8 The thermal melting profile of st-DNA (150 μM) in the presence of **1–3** (P/D 10) in 10 mM phosphate buffer (pH 7.0). (Data for **1** were taken from ref. 10.)

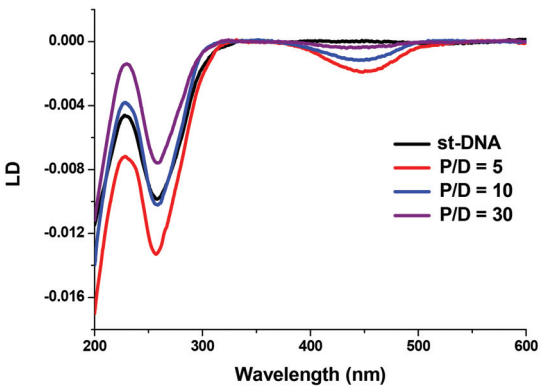

Fig. 9 The LD spectra of st-DNA (400 μM) in the presence of varying concentration of **2** (P/D 0 → 30) in 10 mM phosphate buffer (pH 7.0).

Linear dichroism spectroscopy

The mode of binding of **2** and **3** with st-DNA was investigated using linear dichroism (LD) spectroscopy. As shown in Fig. 9, in the absence of any ligand, a negative LD signal is observed

for st-DNA at λ = 260 nm, characteristic of B-DNA, arising from the nearly perpendicular orientation of the transition moments of DNA bases relative to the DNA helical axis.[28] In the presence of **2**, in addition to the negative LD signal at 260 nm for DNA, a second negative LD signal was observed around 440 nm corresponding to the ICT absorption band of **2**. Due to significant overlap of the DNA absorption band and the absorption band of **2** below 300 nm, a complete quantitative interpretation of the flow linear dichroism data was not possible. However, the presence of a negative LD signal centred at *ca*. 440 nm in the presence of **2** suggests that **2** binds to st-DNA *via* intercalation. The LD spectra of st-DNA in the presence of **3** (ESI†) also showed the appearance of a negative LD band at *ca*. 440 nm. For the 260 nm band corresponding to the transitions of DNA bases, reduced linear dichroism (LD^r) was calculated to be −0.027 ± 0.003, a value similar to that obtained for B-DNA samples by other research groups.[28] In the presence of **2** and **3**, the LD^r values calculated for the 440 nm band and the nucleobase region were found to be −0.032 ± 0.003 and −0.034 ± 0.003 respectively, which are similar to that observed for the DNA bases thereby supporting the conclusion that the naphthalimide ligands lie in the same plane as the DNA bases.

Circular dichroism spectroscopy

CD titrations were carried out by monitoring the conformational changes of st-DNA (150 μM) in the presence of increasing concentrations of the ligand of interest. The CD spectra of st-DNA in the presence of varying concentrations of **2** are shown in Fig. 10 and that in the presence of **3** are shown in ESI.† The molar ellipticity of the positive band at 275 nm band increased significantly in the presence of increasing concentrations of the ligands and showed *ca*. 3 nm red shifts. Notably, no induced CD signal was observed for the bound naphthalimide in any case. An induced signal would be expected if it were groove-bound to the DNA as has previously been reported for the unsubstituted 1,8-naphthalimide.[11] An increase in the molar ellipticity of the CD band of double stranded DNA centred at 275 nm has been previously observed in the case of intercalative binding.[29] These changes along with LD measurements are indicative of the intercalative mode of binding.

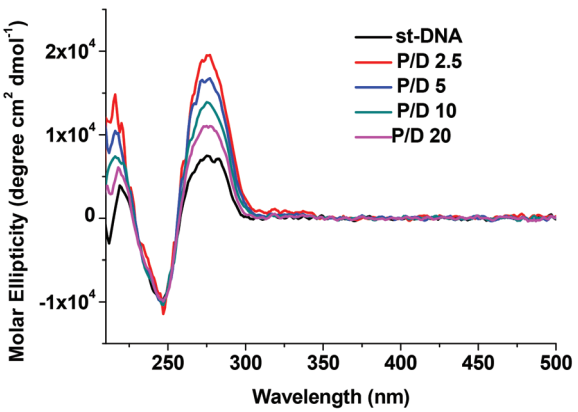

Fig. 10 The CD spectra of st-DNA (150 μM) in the presence of varying concentration of **2** (P/D 0 → 20) in 10 mM phosphate buffer (pH 7.0).

Conclusion

This study shows that the cationic 4-amino-1,8-naphthalimide derivatives **2** and **3** possessing an ethyl pyridinium side chain bind strongly to DNA. Spectroscopic titrations along with linear dichroism measurements suggest that the ligands bind *via* intercalation between the DNA base pairs. The strong stacking interaction between the planar naphthalimide ring and the DNA bases is further confirmed by the titration with 5′-AMP and 5′-GMP. Cationic side chains (such as the methyl pyridinium moiety here) might be expected to interact with the phosphate backbone of the DNA[30] or with the O6 and the N7 atoms of guanine,[31] if the side chain is bound in the major groove.

It is interesting to note that the excited state interaction of **2** with st-DNA is quite different from the previously reported 4-amino-1,8-naphthalimide derivative **1** where the pyridine moiety is bound directly to the ethylene linking group. Compound **2** shows comparable binding affinities to poly(dA–dT)$_2$ and poly(dG–dC)$_2$ whereas compound **1** shows a 6 times greater affinity to the AT-polymer. These differences in behaviour are surprising given the similarity of the two side-chains, and hence, must indicate an unfavourable interaction of the pyridinium group of **1** with either the guanine or cytosine. This could possibly be a steric interaction between this group and the 2-amino group of guanine in the minor groove. It is intriguing to consider whether this steric demand is due to the interaction of the pyridinium group in **1** with the naphthalimide oxygen as found in the crystal structure of **1** and caused the ethylene group to form a *gauche* conformation. This clearly demonstrates that the minor structural changes in the imide substituent can have a major effect on the DNA binding affinity. Another particularly intriguing difference between **1** and **2** is the latter's biphasic fluorescence response with st-DNA (but not with the synthetic polynucleotides). This presumably indicates that there is a change in binding site with the loading of **2** on the DNA, perhaps a preference for a particular sequence. Determination of this will require a study with a defined sequence DNA.

Dimethyl substitution on the amino nitrogen in **3** was found to cause a major reduction of the fluorescence quantum yield of the system in all solvents. The low quantum yield of **3** compared to that observed for the amino analogue **2** has been rationalised in terms of increased non-radiative deactivation pathways induced by the presence of twisted NMe_2 group in **3**. The presence of the dimethyl amino group presumably also interferes with the stacking with 5′-AMP and 5′-GMP as suggested by the reduced binding constant of **3** for both 5′-AMP and 5′-GMP. This study also revealed that **2** and **3** show significantly different excited state interactions with adenine and guanine rich sequences, where the excited singlet state of

the amino derivative is partly quenched in the presence of guanine (the most easily oxidisable base) but not with adenine. This is probably due to the lower reduction potential of the excited state of **2**, and is consistent with the known shift of the ground state potential upon methylation of amino-naphthalimides.[14e]

Each of **1**, **2** and **3** shows enhanced fluorescence in the DNA bound form resulting primarily from the localisation of the chromophore in a rigid, non-polar environment; this translates into almost a 16 fold increase in the quantum efficiency of **3** bound to DNA, which suggests potential use of such a ligand as solvatochromic probes to study DNA/protein structures. We are currently exploring the use of these compounds in greater detail.

General experimental details

All chemicals were obtained from Sigma-Aldrich, Fluka or TCI (Europe) and were used without further purification. Deuterated solvents for NMR were purchased from Apollo Ltd. The mononucleotides 5′-AMP, 5′-GMP, st-DNA and the homopolymeric nucleotides poly(dA–dT)$_2$ and poly(dG–dC)$_2$ were obtained from Sigma-Aldrich as their sodium salts. They were stored at −20 °C to prevent bacterial growth. The DNA concentration per nucleotide was determined spectrophotometrically using the molar extinction coefficients ε_{260} = 6.6 × 10^3 M^{-1} cm^{-1} for st-DNA, ε_{254} = 8.4 × 10^3 M^{-1} cm^{-1} for poly(dG–dC)$_2$ and ε_{260} = 6.6 × 10^3 M^{-1} cm^{-1} for poly(dA–dT)$_2$, respectively.

All NMR spectra were recorded using either a Bruker DPX-400 or AV-600 spectrometer, operating at 400/600 MHz for ^{1}H NMR and 100/150 MHz for ^{13}C NMR, respectively. Chemical shifts were referenced relative to the internal solvent signals. Multiplicities are abbreviated as follows: singlet (s), doublet (d), triplet (t), double triplet (dt). Infrared (IR) spectra were recorded on a Perkin Elmer Spectrum 100 FT-IR spectrophotometer equipped with a Universal ATR sampling accessory. Electrospray mass spectra were recorded on a Micromass LCT spectrometer or a MALDI QToF Premier, running Mass Lynx NT V 3.4 on a Waters 600 controller connected to a 996 photodiode array detector using HPLC grade methanol, water or acetonitrile as carrier solvents. High resolution mass spectra were obtained by a peak matching method using leucine enkephaline (Tyr-Gly-Gly-Phe-Leu) as the reference (m/z = 556.2771). All accurate masses were quoted to ≤5 ppm. Melting points were determined using an Electrothermal IA9000 digital melting point apparatus. Elemental analysis of all compounds was carried out at the Microanalytical Laboratory, School of Chemistry and Chemical Biology, University College Dublin.

X-ray crystallography

X-ray data (Tables S1 and S2†) were collected on either a Rigaku Saturn 724 CCD Diffractometer using graphite-monochromated Mo-Kα radiation (λ = 0.71073 Å) or a Bruker Apex2 Duo using a high intensity Cu-Kα radiation source (λ = 1.54178 Å). The data sets from the Rigaku Saturn-724 diffractometer were collected using Crystalclear-SM 1.4.0 software. Data integration, reduction and correction for absorption and polarisation effects were all performed using Crystalclear-SM 1.4.0 software. Space group determination was obtained using CrystalStructure ver. 3.8 software. Datasets collected on the Bruker Apex2 Duo were processed using Bruker APEXv2011.8-0 software. The structures were solved using direct methods (SHELXS-97) and refined against all F^2 data (SHELXL-97). All H-atoms, except for N–H and O–H protons, were positioned geometrically and refined using a riding model with d(CHaro) = 0.95 Å, U_{iso} = 1.2U_{eq} (C) for aromatic, 0.99 Å, U_{iso} = 1.2U_{eq} (C) for CH_2 and 0.98 Å, and U_{iso} = 1.2U_{eq} (C) for CH_3. N–H and O–H protons were found from the difference map and fixed to the attached atoms with UH = 1.2UX. CCDC no. 924757 and 924758.

UV/vis absorption measurements

UV/vis absorption spectra were recorded on a Varian CARY 50 spectrophotometer. All the spectroscopic measurements were carried out in quartz cuvettes (10 mm × 10 mm). The wavelength range was 200–800 nm with a scan rate of 600 nm min^{-1}. MilliQ water was used in DNA related work. Phosphate buffer: two 1 M stock solutions of Na_2HPO_4 and NaH_2PO_4 were made up with MilliQ water. Portions of each solution were diluted together to achieve 10 mM phosphate buffer of pH 7.0, which was then filtered using a 0.45 μM syringe filter. Baseline corrections were performed for all spectral measurements. All solutions were prepared fresh prior to measurement. The UV/vis titrations were carried out by monitoring the changes in the absorption spectra of the ligand of interest in 10 mM phosphate buffer (pH 7.0) upon gradual addition of mononucleotides/st-DNA/polynucleotides. All the titrations were repeated at least three times to ensure reproducibility.

Fluorescence measurements

Steady-state fluorescence spectra were recorded using a Varian Cary Eclipse spectrofluorimeter. Fluorescence titrations were carried out using optically dilute solutions (absorbance < 0.1) by following the same procedure as described for UV/vis titrations. Fluorescence quantum yields of the 4-amino-1,8-naphthalimide derivatives were calculated using fluorescein in 0.1 N NaOH (ϕ_F = 0.92, λ_{ex} = 436 nm) as the reference.[32] For the determination of the quantum yields, a number of solutions of the ligand with absorbance ranging from 0.02 to 0.1 were used. Optically matched solutions of the samples and reference were used. The fluorescence emission spectra of the samples and the standard were measured under the same experimental settings. The integrated areas under the emission spectra were measured using the in-built software of the spectrofluorimeter. All the quantum yield values reported are within 10% error. Fluorescence lifetimes were measured using a Horiba Jobin Yvon Fluorolog FL 3-22 equipped with a FluoroHub v2.0 single photon controller using the time-correlated single photon counting method (TCSPC), run in reverse mode. The samples were excited with a pulsed nanosecond light-emitting diode (NanoLED®, λ_{ex} = 458 nm). All the decay traces were corrected for the instrument response by recording the scatter signal at an identical excitation/emission wavelength

using a dilute solution of colloidal silica (Ludox®). All the measurements were performed at 298 K. The decay traces were analysed using the in-built IBH DAS6 software of the Fluorolog 3 instrument using a non-linear least-squares error minimisation analysis using eqn (1).

$$I(t) = \sum_{i=1}^{n} \alpha_i \exp\left(\frac{-t}{\tau_i}\right) \quad (1)$$

where α_i represents the pre-exponential factor and τ_i is the fluorescence lifetime.

In the case of a bi-exponential decay, the average fluorescence lifetime was determined using eqn (2)

$$\tau_{av} = \frac{\sum_{i=1}^{n} \alpha_i \tau_i}{\sum_{i=1}^{n} \alpha_i} \quad (2)$$

Circular dichroism and linear dichroism

CD spectra were recorded using a JASCO J810 spectropolarimeter. Each CD trace represents the average of three scans. Linear dichroism spectra were recorded using a JASCO J-815 CD spectropolarimeter equipped with a Dioptica Scientific Ltd linear dichroism accessory. The CD spectra were presented as molar ellipticity using eqn (3).

$$[\theta] = \frac{100\theta}{cl} \quad (3)$$

$[\theta]$ is the molar ellipticity, θ is the ellipticity (in degrees), c is the molar concentration and l is the pathlength (expressed in centimetres). The LD spectra were presented as the average of three scans.

Thermal denaturation assays

Thermal denaturation experiments were conducted using a Perkin-Elmer 35 UV/vis spectrophotometer coupled to a Peltier temperature controller. The temperature was ramped from 30 °C to 90 °C at a rate of 1 °C min^{-1} and the absorbance at 260 nm was measured at 0.2 °C intervals. All the solutions were thoroughly degassed prior to measurement.

Synthesis

***N*-[2-(Pyridin-4-yl)ethyl]-4-nitro-1,8-naphthalimide (5).** 4-Nitro-1,8-naphthalic anhydride (1.674 g, 6.88 mmol) was placed in a round bottom flask along with molecular sieves. To this, 25 mL of anhydrous toluene was added using cannula, followed by the addition of 4-(2-aminoethyl)pyridine (0.83 mL, 6.88 mmol) and triethylamine (1.92 mL, 13.77 mmol) and the reaction mixture was stirred at reflux for 48 h under an argon atmosphere. Upon completion, the mixture was filtered through celite while still hot and washed with toluene. The filtrate was removed under reduced pressure and the resulting brown solid was dissolved in CH_2Cl_2, washed once with a saturated solution of $NaHCO_3$, followed by washing with water and brine, respectively. The organic layer was dried over $MgSO_4$ and excess CH_2Cl_2 was removed under reduced pressure to give **5** as a shiny brown solid in 47% yield (1.13 g) after recrystallisation from ethanol. M.p. 163–163.8 °C; Found: C, 62.81; H, 4.02; N, 11.32%. $C_{19}H_{13}N_3O_4 \cdot 0.9H_2O$ requires C, 62.77; H, 4.10; N, 11.56%; HRMS: Found 348.0980 ($[M + H]^+$, $C_{19}H_{14}N_3O_4$ requires 348.0984). δ_H (400 MHz, $CDCl_3$), 8.84 (1H, d, J = 8.0 Hz, Ar-H5), 8.72 (1H, d, J = 8.0 Hz, Ar-H7), 8.67 (1H, d, J = 8.0 Hz, Ar-H2), 8.52 (2H, d, J = 5.6 Hz, Py-H16), 8.40 (1H, d, J = 8.0 Hz, Ar-H3), 7.99 (t, 1H, J = 8.0 Hz, Ar-H6), 7.28 (2H, d, J = 5.4 Hz, Py-H17), 4.44 (2H, t, J = 8.0 Hz, CH_2), 3.06 (2H, t, J = 8.0 Hz, CH_2). δ_C (100 MHz, $CDCl_3$), 163.2 (C═O), 162.4 (C═O), 149.7 (C), 149.6 (CH), 147.6 (C), 132.6 (CH), 130.0 (CH), 129.8 (CH), 129.6 (CH), 129.1(C), 126.6 (C), 124.4 (CH), 123.9 (CH), 123.7 (C), 122.7 (C), 40.8 (CH_2), 33.8 (CH_2); ν_{max} (neat sample)/cm^{-1}: 2938, 2852, 1702, 1657, 1625, 1595, 1520, 1438, 1410, 1338, 1272, 1233, 1007, 836, 784, 759.

***N*-[2-(Pyridin-4-yl)ethyl]-4-amino-1,8-naphthalimide (4).** Compound **5** (0.65 g, 1.87 mmol) was heated with 10% Pd/C in ethanol at 70 °C for one hour. To this solution, an excess of hydrazine monohydrate (0.9 mL, 18.55 mmol) was added dropwise. The colour of the reaction mixture changed from black to green within a couple of minutes and the mixture was heated for a further 6 h, filtered through celite while hot and washed with ethanol. The combined solvents were removed under reduced pressure and **4** was obtained as a bright yellow solid in 94% yield (0.56 g). M.p. decomposed above 289 °C; HRMS: Found 318.1242 ($[M + H]^+$, $C_{19}H_{16}N_3O_2$ requires 318.1243). δ_H (400 MHz, DMSO-d_6), 8.63 (1H, d, J = 8.0 Hz, Ar-H5), 8.46 (2H, d, J = 5.5 Hz, Py-H16), 8.42 (1H, d, J = 4.0 Hz, Ar-H7), 8.19 (1H, d, J = 8.0 Hz, Ar-H2), 7.66 (1H, t, J = 8.0 Hz, Ar-H6), 7.50 (2H, s, NH_2), 7.29 (2H, d, J = 5.5 Hz, Py-H17), 6.85 (1H, d, J = 8.0 Hz, Ar-H3), 4.27 (2H, t, J = 8.0 Hz, CH_2), 2.94 (2H, t, J = 8.0 Hz, CH_2). δ_C (100 MHz, DMSO-d_6): 164.1 (C═O), 163.2 (C═O), 153.3 (C), 150.0 (CH), 148.3 (C), 134.5 (CH), 131.5 (CH), 130.2 (C), 129.9 (CH), 124.6 (CH), 124.5 (CH), 122.1 (C), 119.8 (C), 108.7 (CH), 107.8 (C), 39.9 (CH_2), 33.4 (CH_2). ν_{max} (neat sample)/cm^{-1}: 3370, 2923, 2852, 1670, 1632, 1612, 1566, 1525, 1481, 1432, 1363, 1350, 1307, 1245, 1131, 826, 774, 759.

***N*-[2-(Methylpyridin-1-ium)ethyl]-4-amino-1,8-naphthalimide (2).** Compound **4** (0.42 g, 1.33 mmol) was suspended in anhydrous acetone and CH_3I (0.83 mL, 13.33 mmol) was added and the reaction mixture was then heated at reflux for 48 h. Upon completion, the resulting precipitate was collected by filtration and washed with CH_2Cl_2. The crude product was converted into its PF_6^- salt and purified by silica flash chromatography using CH_3CN–H_2O–NaCl (saturated) (88 : 11 : 1). The product was precipitated as its PF_6^- salt using a concentrated aqueous solution of ammonium hexafluorophosphate and finally converted to the Cl^- salt using Amberlite IRA 400 (Cl) ion exchange resin in methanol. Excess methanol was removed under reduced pressure and **2** was obtained as a bright yellow solid in 93% yield (0.455 g). M.p. decomposed above 255 °C; Found: C, 61.78; H, 4.68; N, 10.46%. $C_{20}H_{18}ClN_3O_2 \cdot 0.3NaCl \cdot 0.2CH_3OH$ requires C, 61.93; H, 4.84; N, 10.73%; HRMS: Found 333.1474 ($[M + H]^+$, $C_{20}H_{19}N_3O_2$ requires 333.1477). δ_H (600 MHz, DMSO-d_6), 8.85 (2H, d, J = 6.0 Hz, Py-H17), 8.66 (1H, d, J = 8.6 Hz, Ar-H5), 8.41 (1H, d, J = 8.0 Hz, Ar-H7), 8.17 (1H, d, J = 8.4 Hz, Ar-H2), 8.04 (2H, d, J = 6.0 Hz, Py-H16), 7.66

(1H, t, J = 8.0 Hz, Ar-H6), 7.55 (2H, s, NH_2), 6.87 (1H, d, J = 8.5 Hz, Ar-H3), 4.39 (2H, t, J = 7.0 Hz, CH_2), 4.30 (3H, s, CH_3), 3.27 (2H, t, J = 7.0 Hz, CH_2). δ_C (150 MHz), 164.3 (C=O), 163.3 (C=O), 159.5 (C), 153.5 (C), 145.2 (CH), 134.6 (CH), 131.6 (CH), 130.3 (C), 130.2 (CH), 128.3 (CH), 124.5 (CH), 121.9 (C), 119.8 (C), 108.7 (CH), 107.5 (C), 47.7 (CH_3), 39.2 (CH_2), 34.2 (CH_2). ν_{max} (neat sample)/cm^{-1}: 3340, 2932, 2852, 1685, 1669, 1626, 1577, 1526, 1474, 1384, 1343, 1253, 1130, 841, 775, 757.

4-*N*,*N*′-Dimethylamino-1,8-naphthalimide (7).[12] Dimethylamine (5 mL, 40% aqueous solution, excess) and $CuSO_4 \cdot 5H_2O$ (0.12 g, 0.48 mmol) were added to a suspension of 4-bromo-1,8-naphthalic anhydride (2.5 g, 9.00 mmol) in DMF (30 mL). The reaction mixture was stirred under reflux conditions for 12 h under an argon atmosphere. The solvent was removed under reduced pressure and the resulting yellow solid was purified by recrystallisation from hot methanol to yield the desired product as a bright yellow solid in 78% yield (1.70 g). M.p. (203–204) °C (ref. 12, 206 °C); Found: C, 68.63; H, 4.38; N, 5.89%. $C_{14}H_{11}NO_3 \cdot 0.2H_2O$ requires C, 68.68; H, 4.69; N, 5.72%; HRMS: Found 242.0829 ($[M + H]^+$, $C_{14}H_{12}NO_3$ requires 242.0817; δ_H (400 MHz, $CDCl_3$): 8.54 (1H, d, J = 8.0 Hz, Ar-H7), 8.50 (1H, d, J = 8.0 Hz, Ar-H5), 8.42 (1H, d, J = 8.0 Hz, Ar-H2), 7.68 (1H, t, J = 8.0 Hz, Ar-H6), 7.10 (1H, d, J = 8.0 Hz, Ar-H3), 3.21 (s, 6H, $N(CH_3)_2$). δ_C (100 MHz), 161.7 (C=O), 160.7 (C=O), 157.9 (C), 134.9 (CH), 133.1 (CH), 132.9 (CH), 132.8 (C), 124.9 (CH), 124.7 (C), 119.1 (C), 113.1 (CH), 109.2 (C), 44.6 (CH_3). ν_{max} (neat sample)/cm^{-1}: 1753, 1720, 1582, 1568, 1522, 1495, 1393, 1339, 1307, 1186, 1117, 997, 927, 774, 747.

***N*-[2-(Pyridin-4-yl)ethyl]-4-*N*,*N*′-dimethylamino-1,8-naphthalimide (6).** 4-(2-Aminoethyl)pyridine (0.70 mL, 5.87 mmol) and triethylemine (1.20 mL, 8.80 mmol) were added to the suspension of **7** (1.03 g, 4.27 mmol) in anhydrous toluene and the mixture was stirred under reflux for 3 days under an argon atmosphere. The resulting mixture was filtered through celite while still hot and washed with toluene. The solvent was removed under reduced pressure and the resulting solid was dissolved in CH_2Cl_2, washed once with a saturated solution of $NaHCO_3$, followed by washing with water and brine, respectively. The organic layer was dried over $MgSO_4$ and the solvent was removed under reduced pressure. The resulting solid was purified by recrystallisation from hot methanol to yield **6** as a bright yellow solid in 56% yield (0.83 g). M.p. (157.5–158) °C; Found: C, 72.79; H, 5.43; N, 12.09%. $C_{21}H_{19}N_3O_2 \cdot 0.1H_2O$ requires C, 72.65; H, 5.57; N, 12.10%; HRMS: Found 346.1551 ($[M + H]^+$, $C_{21}H_{20}N_3O_2$ requires 346.1551). δ_H (400 MHz, $CDCl_3$), 8.57 (1H, d, J = 8.0 Hz, Ar-H7), 8.53 (2H, d, J = 4.0 Hz, Py-H16), 8.48 (1H, d, J = 8.0 Hz, Ar-H2), 8.46 (1H, d, J = 8.0 Hz, Ar-H5), 7.68 (1H, t, J = 8.0 Hz, Ar-H6), 7.31 (2H, d, J = 4.0 Hz, Py-H17), 7.13 (1H, t, J = 8 Hz, Ar-H3), 4.43 (2H, t, J = 8 Hz, CH_2), 3.14 (s, 6H, $N(CH_3)_2$), 3.06 (2H, t, J = 8 Hz, CH_2). δ_C (100 MHz): 164.5 (C=O), 163.9 (C=O), 157.2 (C), 149.6 (CH), 148.2 (C), 132.8 (CH), 131.4 (CH), 131.1 (CH), 130.3 (C). 125.3 (C), 124.9 (CH), 124.5 (CH), 122.8 (C), 114.5 (C), 113.3 (CH), 44.8 (CH_3), 40.3 (CH_2), 33.6 (CH_2). ν_{max} (neat sample)/cm^{-1}: 2965, 2843, 1685, 1645, 1583, 1569, 1560, 1415, 1383, 1349, 1267, 1241, 1022, 838, 756.

***N*-[2-(Methylpyridin-1-ium)ethyl]-4-*N*,*N*′dimethylamino-1,8-naphthalimide (3).** Compound **6** (0.16 g, 0.46 mmol) was suspended in anhydrous acetone and CH_3I (0.30 mL, 4.82 mmol) was added and the reaction mixture was heated at reflux for 48 h. After completion of the reaction, the precipitate was collected by filtration, dissolved in CH_2Cl_2 and purified by silica flash chromatography using CH_2Cl_2–methanol (85 : 15). The iodide salt of **3** was obtained as an orange solid in 40% (0.09 g) yield after removal of excess solvent under reduced pressure and converted to the Cl^- salt using Amberlite IRA 400 (Cl) ion exchange resin in methanol. M.p. (203.7–204) °C; Found: C, 61.73; H, 6.09; N, 9.69%. $C_{22}H_{22}ClN_3O_2 \cdot 1.8H_2O$ requires C, 61.69; H, 6.02; N, 9.81%; HRMS: Found 361.1794 ($[M + H]^+$, $C_{22}H_{23}N_3O_2$ requires 361.1790); δ_H (600 MHz, DMSO-d_6), 8.87 (2H, d, J = 6.0 Hz, Py-H17), 8.54 (1H, d, J = 8.5 Hz, Ar-H5), 8.45 (1H, d, J = 8.0 Hz, Ar-H7), 8.32 (1H, d, J = 8.5 Hz, Ar-H2), 8.07 (2H, d, J = 6.0 Hz, Py-H16), 7.77 (1H, t, J = 8.0 Hz, Ar-H6), 7.22 (1H, d, J = 8.0 Hz, Ar-H3), 4.41 (2H, t, J = 7.0 Hz, CH_2), 4.27 (3H, s, CH_3), 3.28 (2H, t, J = 7.0 Hz, CH_2), 3.10 (6H, s, $N(CH_3)_2$). δ_C (150 MHz), 164.0 (C=O), 163.2 (C=O), 159.2 (C), 156.9 (C), 144.8 (CH), 132.7 (CH), 132.0 (CH), 130.9 (CH), 130.0 (C), 128.0 (CH), 125.2 (CH), 124.2 (C), 122.2 (C), 113.0 (CH), 112.9 (C), 47.4 (CH_3), 44.5 ($N(CH_3)_2$), 39.3 (CH_2), 33.6 (CH_2). ν_{max} (neat sample)/cm^{-1}: 2913, 2834, 1693, 1638, 1589, 1574, 1518, 1449, 1395, 1371, 1347, 1264, 1234, 1124, 836, 779, 755.

Acknowledgements

Financial support from Science Foundation Ireland (SFI) for RFP 2006, RFP 2007, RFP 2009, and PI 2010 grants and PRTLI for Cycle 4 funding to CSCB is acknowledged. JAK thanks IRCSET for a postdoctoral fellowship. We would like to thank particularly Dr John O'Brien and Dr Martin Feeney for their help with NMR and MS, respectively.

References

1 S. Banerjee, E. B. Veale, C. M. Phelan, S. A. Murphy, G. M. Tocci, L. J. Gillespie, D. O. Frimannsson, J. M. Kelly and T. Gunnlaugsson, *Chem. Soc. Rev.*, 2013, **42**, 1601.

2 (*a*) S. Neidle and D. E. Thurston, *Nat. Rev. Cancer*, 2005, **5**, 285; (*b*) K. Ninomiya, H. Satoh, T. Sugiyama, M. Shinomiya and R. Kuroda, *Chem. Commun.*, 1996, 1825; (*c*) R. B. P. Elmes, M. Erby, S. M. Cloonan, S. J. Quinn, C. D. Williams and T. Gunnlaugsson, *Chem. Commun.*, 2011, **47**, 686; (*d*) M. F. Braña, J. M. Castellano and M. Morán, *Anti-Cancer Drug Des.*, 1993, **8**, 257; (*e*) P. F. Bousquet, M. F. Braña, D. Conlon, K. M. Fitzgerald, D. Perron, C. Cocchiaro, R. Miller, M. Moran, J. George, X.-D. Qian, G. Keilhauer and C. A. Romerdahl, *Cancer Res.*, 1995, **55**, 1176; (*f*) M. F. Braña, M. Cacho, A. Ramos, M. Teresa Dominguez, J. M. Pozuelo, C. Abradelo, M. Fernanda Rey-Stolle, M. Yuste, C. Carrasco and

C. Bailly, *Org. Biomol. Chem.*, 2003, **1**, 648; (*g*) C. Bailly, C. Carrasco, A. Joubert, C. Bal, N. Wattez, M.-P. Hildebrand, A. Lansiaux, P. Colson, C. Houssier, M. Cacho, A. Ramos and M. F. Braña, *Biochemistry*, 2003, **42**, 4136; (*h*) I. Ott, Y. Xu, J. Liu, M. Kokoschka, M. Harlos, W. S. Sheldrick and X. Qian, *Bioorg. Med. Chem.*, 2008, **16**, 7107; (*i*) Q. Yang, P. Yang, X. Qian and L. Tong, *Bioorg. Med. Chem. Lett.*, 2008, **18**, 6210; (*j*) X. Qian, Y. Li, Y. Xu, Y. Liu and B. Qu, *Bioorg. Med. Chem. Lett.*, 2004, **14**, 2665; (*k*) A. Wu, Y. Xu and X. Qian, *Bioorg. Med. Chem.*, 2009, **17**, 592; (*l*) Z. Chen, X. Liang, H. Zhang, H. Xie, J. Liu, Y. Xu, W. Zhu, Y. Wang, X. Wang, S. Tan, D. Kuang and X. Qian, *J. Med. Chem.*, 2010, **53**, 2589; (*m*) L. Xie, J. Cui, X. Qian, Y. Xu, J. Liu and R. Xu, *Bioorg. Med. Chem.*, 2011, **19**, 961; (*n*) X. Liang, K. Xu, Y. Xu, J. Liu and X. Qian, *Toxicol. Appl. Pharmacol.*, 2011, **256**, 52; (*o*) X. Li, Y. Lin, Y. Yuan, K. Liu and X. Qian, *Tetrahedron*, 2011, **67**, 2299; (*p*) Z.-Y. Tian, S.-Q. Xie, Y.-W. Du, Y.-F. Ma, J. Zhao, W.-Y. Gao and C.-J. Wang, *Eur. J. Med. Chem.*, 2009, **44**, 393; (*q*) Q. Yang, X. Qian, J. Xu, Y. Sun and Y. Li, *Bioorg. Med. Chem.*, 2005, **13**, 1615; (*r*) S.-Q. Xie, Y.-H. Zhang, Q. Li, F.-H. Xu, J.-W. Miao, J. Zhao and C.-J. Wang, *Apoptosis*, 2012, **17**, 725.

3 R. M. Duke, E. B. Veale, F. M. Pfeffer, P. E. Kruger and T. Gunnlaugsson, *Chem. Soc. Rev.*, 2010, **39**, 3936.

4 (*a*) E. B. Veale, J. A. Kitchen and T. Gunnlaugsson, *Supramol. Chem.*, 2013, **25**, 101; (*b*) T. Gunnlaugsson, T. C. Lee and R. Parkesh, *Org. Biomol. Chem.*, 2003, **1**, 3265; (*c*) T. Gunnlaugsson, P. E. Kruger, T. C. Lee, R. Parkesh, F. M. Pfeffer and G. M. Hussey, *Tetrahedron Lett.*, 2003, **44**, 6575; (*d*) F. M. Pfeffer, A. M. Buschgens, N. W. Barnett, T. Gunnlaugsson and P. E. Kruger, *Tetrahedron Lett.*, 2005, **46**, 6579.

5 A. P. de Silva, H. Q. N. Gunaratne and T. Gunnlaugsson, *Tetrahedron Lett.*, 1998, **39**, 5077.

6 R. Parkesh, T. Clive Lee and T. Gunnlaugsson, *Tetrahedron Lett.*, 2009, **50**, 4114.

7 (*a*) G. J. Ryan, S. Quinn and T. Gunnlaugsson, *Inorg. Chem.*, 2007, **47**, 401; (*b*) G. J. Ryan, R. B. P. Elmes, S. J. Quinn and T. Gunnlaugsson, *Supramol. Chem.*, 2012, **24**, 175.

8 (*a*) E. B. Veale, D. O. Frimannsson, M. Lawler and T. Gunnlaugsson, *Org. Lett.*, 2009, **11**, 4040; (*b*) E. B. Veale and T. Gunnlaugsson, *J. Org. Chem.*, 2010, **75**, 5513.

9 R. B. P. Elmes, M. Erby, S. A. Bright, D. C. Williams and T. Gunnlaugsson, *Chem. Commun.*, 2012, **48**, 2588.

10 S. Banerjee, J. A. Kitchen, T. Gunnlaugsson and J. M. Kelly, *Org. Biomol. Chem.*, 2012, **10**, 3033.

11 S. McMasters and L. A. Kelly, *Photochem. Photobiol.*, 2007, **83**, 889.

12 K. J. Kilpin, C. M. Clavel, F. Edafe and P. J. Dyson, *Organometallics*, 2012, **31**, 7031.

13 B. L. Schottel, H. T. Chifotides and K. R. Dunbar, *Chem. Soc. Rev.*, 2008, **37**, 68.

14 (*a*) A. Pardo, J. M. L. Poyato, E. Martin, J. J. Camacho, D. Reyman, M. F. Braña and J. M. Castellano, *J. Photochem. Photobiol., A*, 1989, **46**, 323; (*b*) A. Pardo, J. M. L. Poyato, E. Martin, J. J. Camacho and D. Reyman, *J. Lumin.*, 1990, **46**, 381; (*c*) E. Martín, J. L. G. Coronado, J. J. Camacho and A. Pardo, *J. Photochem. Photobiol., A*, 2005, **175**, 1; (*d*) D. Yuan and R. G. Brown, *J. Phys. Chem. A*, 1997, **101**, 3461; (*e*) S. Saha and A. Samanta, *J. Phys. Chem. A*, 2002, **106**, 4763; (*f*) S. Saha and A. Samanta, *J. Phys. Chem. A*, 1998, **102**, 7903.

15 (*a*) P. Kucheryavy, G. F. Li, S. Vyas, C. Hadad and K. D. Glusac, *J. Phys. Chem. A*, 2009, **113**, 6453; (*b*) T. Soujanya, R. W. Fessenden and A. Samanta, *J. Phys. Chem.*, 1996, **100**, 3507.

16 V. Thiagarajan, C. Selvaraju, E. J. P. Malar and P. Ramamurthy, *ChemPhysChem*, 2004, **5**, 1200.

17 (*a*) J. E. Rogers, S. J. Weiss and L. A. Kelly, *J. Am. Chem. Soc.*, 2000, **122**, 427; (*b*) S. McMasters and L. A. Kelly, *J. Phys. Chem. B*, 2006, **110**, 1046.

18 (*a*) G. Scatchard, *Proc. New York Acad. Sci.*, 1949, **51**, 660; (*b*) D. A. Deranleau, *J. Am. Chem. Soc.*, 1969, **91**, 4044.

19 (*a*) I. V. Sazanovich, E. P. Petrov and V. S. Chirvony, *Opt. Spectrosc.*, 2006, **100**, 209; (*b*) V. S. Chirvony, V. A. Galievsky, N. N. Kruk, B. M. Dzhagarov and P. Y. Turpin, *J. Photochem. Photobiol., B*, 1997, **40**, 154.

20 C. Prunkl, M. Pichlmaier, R. Winter, V. Kharlanov, W. Rettig and H.-A. Wagenknecht, *Chem.–Eur. J.*, 2010, **16**, 3392.

21 K. A. Stevenson, S. F. Yen, N. C. Yang, D. W. Boykin and W. D. Wilson, *J. Med. Chem.*, 1984, **27**, 1677.

22 J. D. McGhee and P. H. von Hippel, *J. Mol. Biol.*, 1974, **86**, 469.

23 E. Tuite and J. M. Kelly, *Biopolymers*, 1995, **35**, 419.

24 Y. Li, Y. Xu, X. Qian and B. Qu, *Tetrahedron Lett.*, 2004, **45**, 1247.

25 (*a*) C. Hiort, P. Lincoln and B. Norden, *J. Am. Chem. Soc.*, 1993, **115**, 3448; (*b*) C. Moucheron, A. Kirsch-De Mesmaeker and S. Choua, *Inorg. Chem.*, 1997, **36**, 584.

26 (*a*) G. Loving and B. Imperiali, *J. Am. Chem. Soc.*, 2008, **130**, 13630; (*b*) G. Loving and B. Imperiali, *Bioconjugate Chem.*, 2009, **20**, 2133; (*c*) B. N. Goguen, G. S. Loving and B. Imperiali, *Bioorg. Med. Chem. Lett.*, 2011, **21**, 5058.

27 M. Cory, D. D. McKee, J. Kagan, D. W. Henry and J. A. Miller, *J. Am. Chem. Soc.*, 1985, **107**, 2528.

28 (*a*) B. Nordén, A. Rodger and T. Dafforn, *Linear Dichroism and Circular Dichroism*, The Royal Society of Chemistry, 2010; (*b*) E. Tuite and B. Nordén, *Bioorg. Med. Chem.*, 1995, **3**, 701.

29 A. Rajendran and B. U. Nair, *Biochim. Biophys. Acta, Gen. Subj.*, 2006, **1760**, 1794.

30 (*a*) A. Rajendran, V. Thiagarajan, B. Rajendar, S. Nishizawa and N. Teramae, *Biochim. Biophys. Acta, Gen. Subj.*, 2009, **1790**, 95; (*b*) A. Rajendran, C. Zhao, B. Rajendar, V. Thiagarajan, Y. Sato, S. Nishizawa and N. Teramae, *Biochim. Biophys. Acta, Gen. Subj.*, 2010, **1800**, 599.

31 (*a*) V. Thiagarajan, A. Rajendran, H. Satake, S. Nishizawa and N. Teramae, *ChemBioChem*, 2010, **11**, 94; (*b*) A. K. Todd, A. Adams, J. H. Thorpe, W. A. Denny, L. P. G. Wakelin and C. J. Cardin, *J. Med. Chem.*, 1999, **42**, 536; (*c*) B. Gold, *Biopolymers*, 2002, **65**, 173.

32 G. A. Crosby and J. N. Demas, *J. Phys. Chem.*, 1971, **75**, 991.